ARTICLE

Jian-Wei Li · Mei-Fu Zhou · Xian-Fu Li
Zi-Jin Li · Zhao-Ren Fu

Origin of a large breccia-vein system in the Sanerlin uranium deposit, southern China: a reinterpretation

Abstract The early Tertiary Sanerlin uranium deposit is located near the southwestern margin of the Chaling–Yongxing pull-apart basin defined by the Chaling–Yongxing and Chenxian–Linwu sinistral strike-slip faults in southern China. The uranium ores are hosted in 15 breccia-vein bodies, which are separately located in the cores of three secondary anticlines of the Upper Permian Dangchong Formation. Individual breccia-vein bodies are composed of fragments of silicified shale and sandstone from the Dangchong Formation, and quartz veinlets as cements. These fragments, together with quartz veins, form a mosaic texture. Hydrothermal pitchblende is the only commercial uranium mineral, mainly occurring as disseminated grains within quartz veins or coating fragments. Other metallic minerals include molybdenite, pyrite, chalcopyrite, galena, sphalerite, and red microcrystalline hematite. Fluid inclusions in quartz veins have homogenization temperatures ranging from 150 to 280 °C, and calculated salinity values between 5.6 and 13.4 wt% NaCl equivalent. Stable isotope analyses show that the mineralizing fluid was characterized by $\delta^{18}O$ values of –2.2 to +2.6‰ and δD_{H_2O} values of –134 to –110‰. These analytical data demonstrate that hydrothermal fluids were mainly derived from formation waters (brines) of the Chaling–Yongxing basin. Fluid overpressuring was caused by an abnormal geothermal gradient and impermeable shales in the deposit area. The geometry, texture, and structure of the breccia-vein system, along with the fluid pressure estimates, suggest that hydraulic fracturing generated the mineralized breccia-vein system. Pitchblende and associated minerals were deposited when gaseous phases were released abruptly from the ore fluids due to the hydraulic fracturing.

J.-W. Li (✉) · X.-F. Li · Z.-J. Li · Z.-R. Fu
Faculty of Earth Resources,
China University of Geosciences,
Wuhan 430074, China
E-mail: jianwei_li@hotmail.com

M.-F. Zhou
Department of Earth Sciences,
The University of Hong Kong,
Hong Kong, China

Introduction

Previous studies demonstrate that hydraulic fracturing is one of the most common and important fluid-assisted types of brittle deformation (Hubbert and Willis 1957; Fyfe et al. 1978; Ramsay 1980; Etheridge et al. 1983; Cox 1995). A variety of hydrothermal ore deposits are associated with hydrothermally cemented breccias (Sillitoe 1985; Sibson 1987). Some mineralized breccias are thought to have undergone a two-stage formation: early fracturing of rocks and later hydrothermal activity within these fractures facilitated by the enhanced permeability (Henley and Adams 1992; Bouchot et al. 1994). However, other investigations suggest that the hydrothermal fluids themselves play a significant role in producing the fractures and breccias, as well as the associated mineralization (Phillips 1972; Callan and Spooner 1998). A few studies have proposed that some hydrothermal uranium deposits and their host breccias were produced simultaneously by hydraulic fracturing (Gauthier-Lafaye and Weber 1989; Mathis et al. 1990).

This paper reports the first example from China of a large tonnage uranium deposit, the Sanerlin deposit, formed by hydraulic fracturing and reinterprets its origin. This deposit was discovered in the late 1950s during an airborne radiometric survey, followed by detailed studies of anomalies. It was subsequently developed from the early 1960s to the middle 1990s and has produced more than 10,000 tonnes of U_3O_8, making it one of the most important uranium deposits in China.
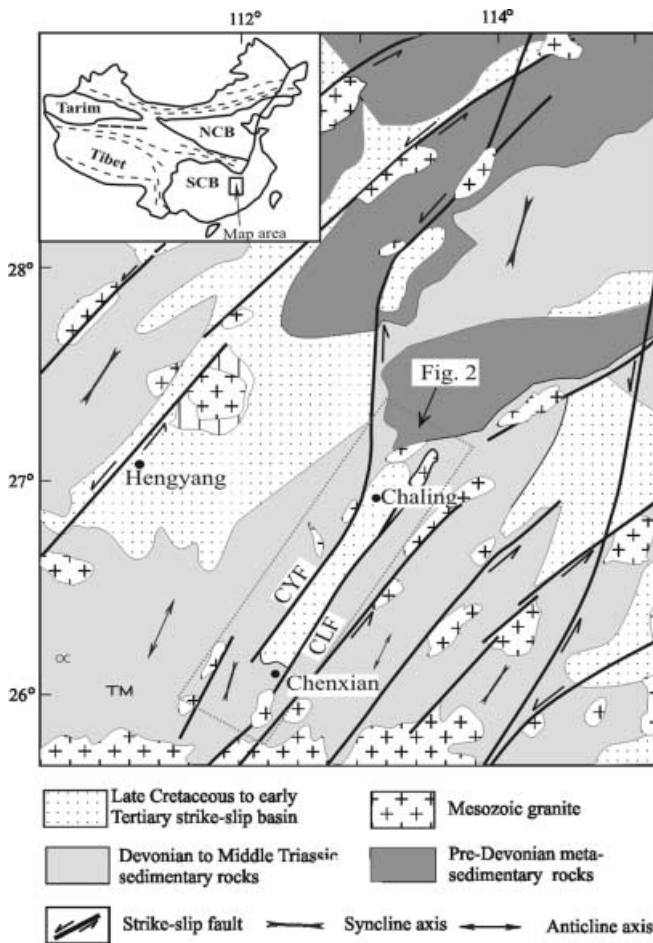
214

Fig. 1 Tectonic setting of the study area showing the NNE-trending strike-slip faults, the folds of Devonian–Middle Triassic sedimentary rocks and the Cretaceous–Tertiary basins. The strike-slip faults were transpressive in Early–Middle Jurassic and transtensional during the Cretaceous–early Tertiary, resulting in the emplacement of Mesozoic granites and formation of pull-apart basins, respectively. *NCB* North China block, *SCB* South China block, *CYF* Chaling–Yongxing fault, *CLF* Chenxian–Linwu fault

Uranium ore bodies in the Sanerlin deposit occur exclusively in a giant breccia-vein system exposed over a vertical extent of 700 m. In this paper, we integrate all available geological, geometric, and textural data from the uraniferous breccia-vein system and document its formation by hydraulic fracturing. The origin of the uranium deposit is also discussed in the light of new fluid inclusion and stable isotope data.
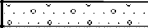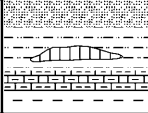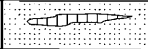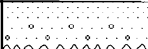
Geological setting

The Sanerlin uranium deposit is located in the South China block (or Yangtze craton), an important part of western Pacific margin of China (Hsü et al. 1990; Gilder et al. 1996). Much of the Mesozoic–Cenozoic geology of the South China block can be related to the oblique subduction of the Pacific plate beneath the eastern part of China (Xu et al. 1987; Li et al. 2001). This subduction has resulted in the formation of NNE-trending Jurassic folds of Devonian to Middle Triassic sedimentary rocks, which overlie the craton basement, together with a large sinistral strike-slip fault system, including the Chaling–Yongxing and Chenxian–Linwu faults in the study area (Fig. 1). The strike-slip fault system in southern China was characterized by transpression in the Early and Middle Jurassic and by transtension from the Late Jurassic to early Tertiary. Granitic intrusions and the regional folds resulted from the transpression, whereas en echelon pull-apart basins developed during the 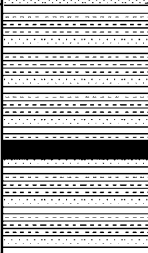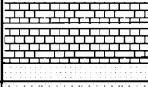later tectonism (Li et al. 2001; Fig. 1). The strike-slip fault system also coincides with a northeastern alignment of more than 100 hot springs, including those in the Sanerlin area, which form one of the largest concentrations of springs in China. They reflect a major thermal anomaly with the groundwater flow being controlled by the regional strike-slip fault system.

The Sanerlin uranium deposit occurs in the pull-apart stepover between the Chaling–Yongxing and Chenxian–Linwu strike-slip faults, near the southern margin of the Chaling–Yongxing basin (Fig. 2). The Chaling–Yongxing basin is filled by about 5,000 m of Cretaceous–Tertiary sedimentary rocks, known as the ''Red Beds'' in China. The red beds, including sandstone, conglomerate, siltstone, gypsum layers, and minor muddy limestone, can be subdivided into five formations (Fig. 3). Granitic intrusions crop out 20–30 km south, as well as north, of the Sanerlin deposit (Fig. 2). Intrusive relationships with strata as young as Middle Triassic and K–Ar and Rb–Sr geochronological data (HB 1988; Jahn et al. 1990) indicate that these granitic rocks are about 140 Ma in age. A geophysical survey substantiates the existence of a granitic batholith beneath the ore bodies (Rao 1993), which has

Fig. 2 Simplified geological map of the Sanerlin area showing the location of the Sanerlin uranium deposit and its spatial relationship to the strike-slip faults, pull-apart basin, and folds. For map area and abbreviations see Fig. 1
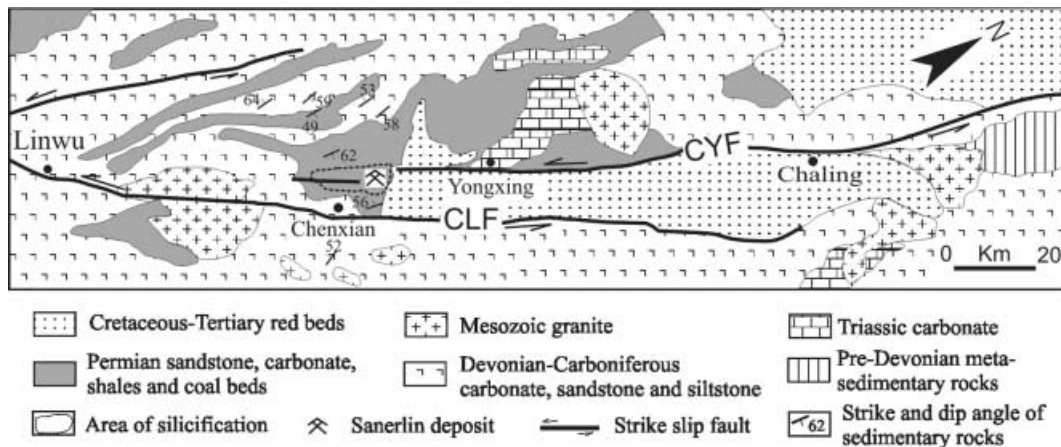
Age	Formation	Stratigraphic column	Thickness (m)	Lithologic description	Uranium abundance (ppm) *
Tertiary	Maoping Formation		20	Fluvial deposits	
Tertiary	Zaoshi Formation		496	Mud-bearing siltstone and sandy marl with thin gypsum lens	$\frac{2.6-4.9}{3.2(9)}$
Cretaceous	Daijia Formation		1500	Conglomerate, coarse to fine sandstone, limestone, mud-bearing siltstone, with seven gypsum beds. These rocks with a red appearence are called "Red Beds".	$\frac{2.1-4.1}{2.9(10)}$
Cretaceous	Shenhuang Formation		975		$\frac{2.5-6.1}{3.4(17)}$
Cretaceous	Dongjing Fortmation		1830		$\frac{3.8-4.9}{4.1(14)}$
Upper Permian	Douling Formaiton		360	Sandstone with thin muddy siltstone and shales	$\frac{2.2-6.5}{3.6(16)}$
Upper Permian	Dangchong Formation		900	Interstratified black shales and quartz sandstone with thin coal beds. The shales are carbonaceous and organic-rich. There are nine shale layers	$\frac{8.7-180.0}{34(118)}$
Lower Permian	Xixia Formation		227	Limestone and dolostone with fine-grained sandstone at the bottom and top	$\frac{2.3-7.2}{4.5(11)}$
	Devonian-Carboniferous		460	Sandstone, siltstone, muddy limestone and minor dolostone	$\frac{3.9-10.2}{5.6(17)}$

Note: * $\frac{\text{Minimum-maximum}}{\text{Average (number of samples)}}$

Fig. 3 General stratigraphic column of the rocks in the area of the Sanerlin deposit. The high content of uranium in rocks of the Dangchong Formation indicates its potential as a source rock for the uranium in the ores. The lithology of the Dangchong Formation is favorable for pre-enrichment of uranium by adsorption and reduction and for developing an impermeable seal

been interpreted as being genetically associated with the surrounding ~140 Ma intrusions.

The stratigraphic sequence in the Sanerlin area includes Devonian, Carboniferous, Permian, and Middle Triassic strata as well as the Cretaceous–Tertiary red beds (Fig. 3). The Devonian to Carboniferous strata consist of sandstone, siltstone, muddy limestone and minor dolostone. The Permian strata include the Xixia, Dangchong, and Douling Formations. The Xixia Formation is composed of limestone and sandstone, which are overlain conformably by rocks of the Dangchong Formation. Rocks of the Douling Formation conformably overly those of the Dangchong Formation and consist mainly of sandstone.

The Dangchong Formation, the major host of the Sanerlin uranium deposit, consists of more than 800 m of very fine-grained quartz sandstone and black siliceous and carbonaceous shales with intercalated coal beds. There are nine black shale layers within the Dangchong Formation, individually ranging from 15 to 42 m in thickness (Fig. 3). These shales contain illite, chlorite, biotite, muscovite, pyrite, and quartz, and are rich in organic materials including algae, organic carbon, lignite, and coal. The shales and sandstones of the Dangchong Formation have been intensely silicified within the mining area (Fig. 2).

The Sanerlin breccia-vein system

The breccia-vein system in Sanerlin is located in the cores of three NNE-trending secondary anticlines belonging to a regional syncline (Figs. 2 and 4). Fifteen breccia bodies form three discontinuous belts striking ~030° within the anticline noses (Fig. 4). Individual breccia bodies are elliptical, commonly 1,000 to 2,000 m long and 100 to 250 m wide, and a majority of the mineralized breccia-vein bodies are restricted to rocks of the Dangchong Formation (Figs. 4 and 5). The intensity of fracturing and brecciation increases from the margins to the centers of individual breccia-vein bodies. Most breccia bodies have a vertical extent of about 700 m (Fig. 5). They are composed of fragments of gray–black silicified shale and sandstone belonging to the Dangchong Formation (Fig. 6A–D). The fragments range from a few millimeters to several meters across and are mainly angular to sub-angular, cemented by quartz veinlets and locally by calcite, which produces a spectacular jigsaw-puzzle pattern in the rock (Fig. 6B, C, D). Few fragments show significant displacement, abrasion or rotation (Fig. 6B and D).

The quartz veins vary from millimeters to more than 30 m in length and from less than 1 cm to about 20 cm in
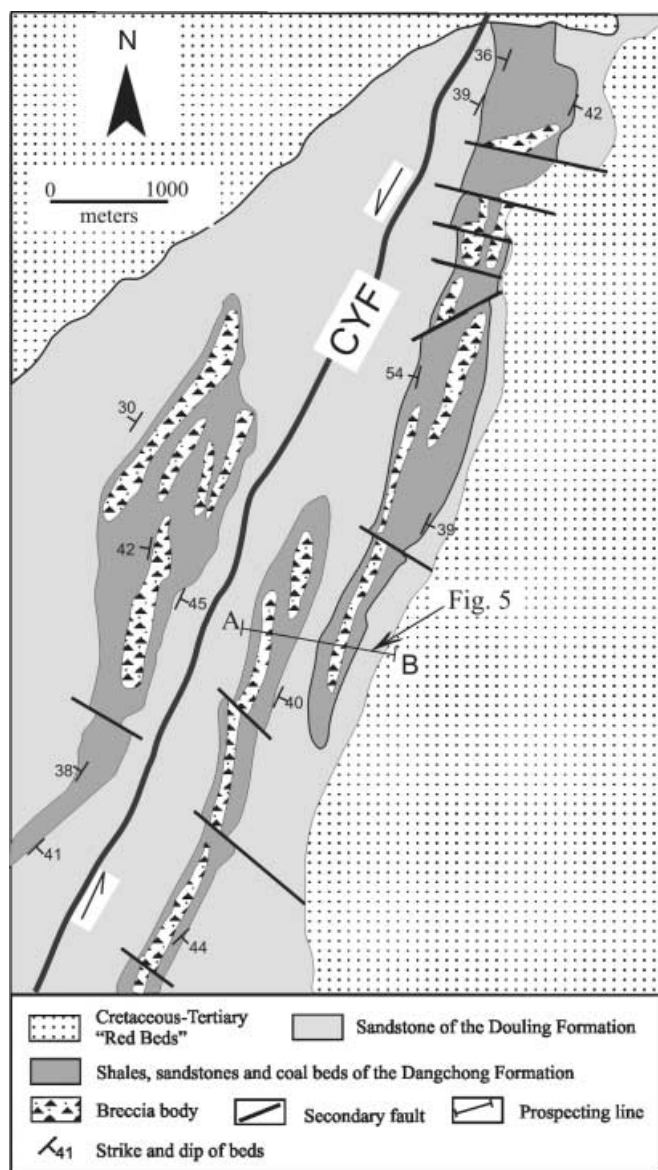
Fig. 4 Plan view of the surface geology of the breccias, showing the possible control of three secondary anticlines on the distribution of the breccia bodies. All breccias are strata bound in rocks of the Dangchong Formation

width. They are commonly characterized by early, very fine-grained silica intergrown with fine-grained pyrite and marcasite. This material cements wall-rock fragments and coats vein walls. This was followed by deposition of crystalline and relatively coarse quartz, with progressively increasing grain size towards the center of the veins (Fig. 6C). Both pitchblende-bearing and pitchblende-free (barren) veins are present. The two types of veins are very similar in appearance and geometry, but crosscutting relationships indicate that the barren veins formed earlier than the uraniferous veins. The quartz veins may be straight, slightly curved, zigzag, branching (horse-tail), or en echelon in form. Many of the veins

contain angular to sub-angular blocks of wall rock ranging from 0.2 to 5 cm in diameter (Fig. 6B and D).

The fragments and hydrothermal cements within the breccia-vein bodies contain many voids and cavities ranging from 0.1 to 5 cm in diameter (Fig. 6B). There is a clear correlation between the void abundance and the size and roundness of the fragments: the more abundant the voids, the smaller and more rounded the fragments.

Wall-rock alteration and uranium ores

Hydrothermal alteration in the Sanerlin deposit is relatively simple. The most important alteration in the area is pervasive and intense silicification. Rocks adjacent to the uranium-bearing quartz veinlets also show abundant pyritization, carbonatization, sericitization, and hematitization. Field and petrographic investigations suggest that the pervasive silicification pre-dated the brecciation. The alteration styles show some variation with depth. At deep levels, detrital albite and microcline contained in rocks of the Dangchong Formation were altered to sericite that is intergrown with quartz and disseminated very fine-grained pyrite, whereas at higher levels the wall rocks are much less altered, pyrite content in the vein decreases, sericite is absent, and the alteration is mainly represented by a few millimeter-wide envelopes of crystalline hematite.

The majority of uranium ores are composed of uraniferous quartz veins and fragments of silicified rocks of the Dangchong Formation. Uranium ore bodies are lenticular, nested, columnar, and irregular. The average uranium content of the ores (186 samples) is 0.54 wt% and most of the ores also contain impurities, which include as much as 525 ppm Mo, 196 ppm Zn, 126 ppm As, 44 ppm Pb, and 253 ppm Cu (Liu 1980). However, unlike many sandstone- and black shale-hosted uranium deposits (Spirakis and Pierson 1986; Dahlkamp 1993), the Sanerlin deposit does not have V enrichment associated with the uranium mineralization.

The primary uranium-bearing mineral, pitchblende, commonly shows sooty, framboidal, colloform, and boytryoidal textures (Fig. 6E and F). It is mainly disseminated in quartz veins or occurs in fragments of wall rock, and locally coats the fragments. The pitchblende grains range from 0.01 to 0.6 mm in diameter and may be fractured or broken (Fig. 6F). A few veinlets of pitchblende, ranging from 0.05 to 2 mm wide and from 0.5 cm to tens of centimeters in length, have also been identified. Molybdenite is widely present in the deposit and locally forms economic ore bodies. Molybdenum grades increase with depth, whereas uranium grades decrease. Other associated metallic minerals include pyrite, marcasite, sphalerite, galena, and minor greenockite, vaesite, chalcopyrite, and red microcrystalline hematite. Gangue minerals are dominantly quartz (chalcedony) and carbonate, with minor fluorite, illite, sericite, and hydromica.
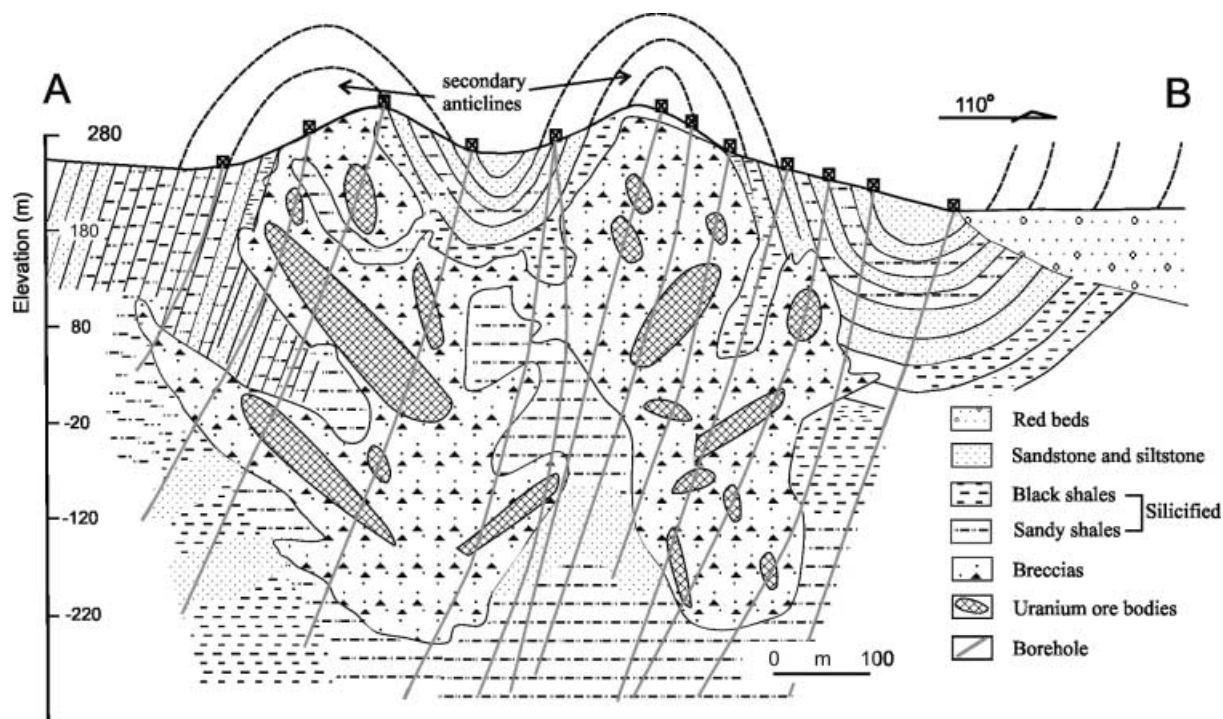
Fig. 5 Representative cross section showing the vertical distribution of the breccia bodies. Note that the breccia bodies occur in the cores of anticlines and most are located in the Dangchong Formation. All of the uranium ore bodies are within the breccias. See Fig. 4 for the location of the cross section

Three stages of mineralization are recognized (Fig. 7). Stage 1 is represented by an assemblage of quartz and sulfide minerals, which include molybdenite, fine-grained pyrite, and chalcopyrite. Pitchblende, accompanied by galena, sphalerite, relatively coarse pyrite, red microcrystalline hematite, and quartz, fluorite, calcite, and hydromica, formed stage 2. Stage 3 mainly involved the formation of minor amounts of gangue minerals and crystalline hematite.

Ores within about 20 m of the surface were oxidized to uranophane, uranopilite, torbernite, zeunerite, and limonite. These supergene minerals indicate paleoclimatic environments conducive to chemical weathering after late Tertiary erosion had exposed the uppermost part of the ore bodies. However, there is no reported economic enrichment of secondary uranium minerals.

Fluid inclusions

General description

Fluid inclusion studies were performed on 19 doubly polished thin sections (0.1–0.4 mm thick) of both pitchblende-barren (stage 1) and pitchblende-bearing quartz veins (stage 2), using a normal petrographic microscope and a Linkam TH600 heating–freezing stage. Inclusions occurring in non-planar, randomly distributed clusters

and as isolated individuals with negative crystal faces were regarded as primary, whereas those outlining healed fractures and planar groups of inclusions were considered to be secondary. Inclusions that have a linear trace, but terminate at the boundary of the host crystal, were interpreted as pseudosecondary according to the criteria of Roedder (1984). For simplicity, both the secondary and pseudosecondary inclusions of Roedder are called secondary in this paper.

Both primary and secondary inclusions are common in quartz veins in the Sanerlin deposit. However, few fluid inclusions are preserved in the early very fine-grained silica that initially cemented the breccia fragments and coats the veins walls. Most primary inclusions are roughly ellipsoidal or elongate with negative crystal faces and, to a lesser extent, irregular in form. A majority of primary and secondary inclusions in the Sanerlin deposit are relatively small, with diameters of about 3–7 μm. However, a few large inclusions have been observed in primary (10 to 30 μm in length) and secondary (8 to 15 μm in length) clusters (Fig. 6F). Only these larger inclusions were amenable to microthermometric studies. The fluid inclusion data from these studies are presented in Table 1.

At room temperature, most primary inclusions are two phases with a vapor bubble varying from 10 to 60% of the inclusion volume. Single phase liquid and vapor inclusions have been observed in rare cases. Secondary inclusions, however, are vapor-dominated, characterized by a vapor bubble that generally exceeds 70% of the inclusion volume. The latter generally lie along planes, known as Tuttle's planes (Tuttle 1949), whose orientations are not dictated by the crystallographic axes of the quartz crystals, but are parallel to microfractures that
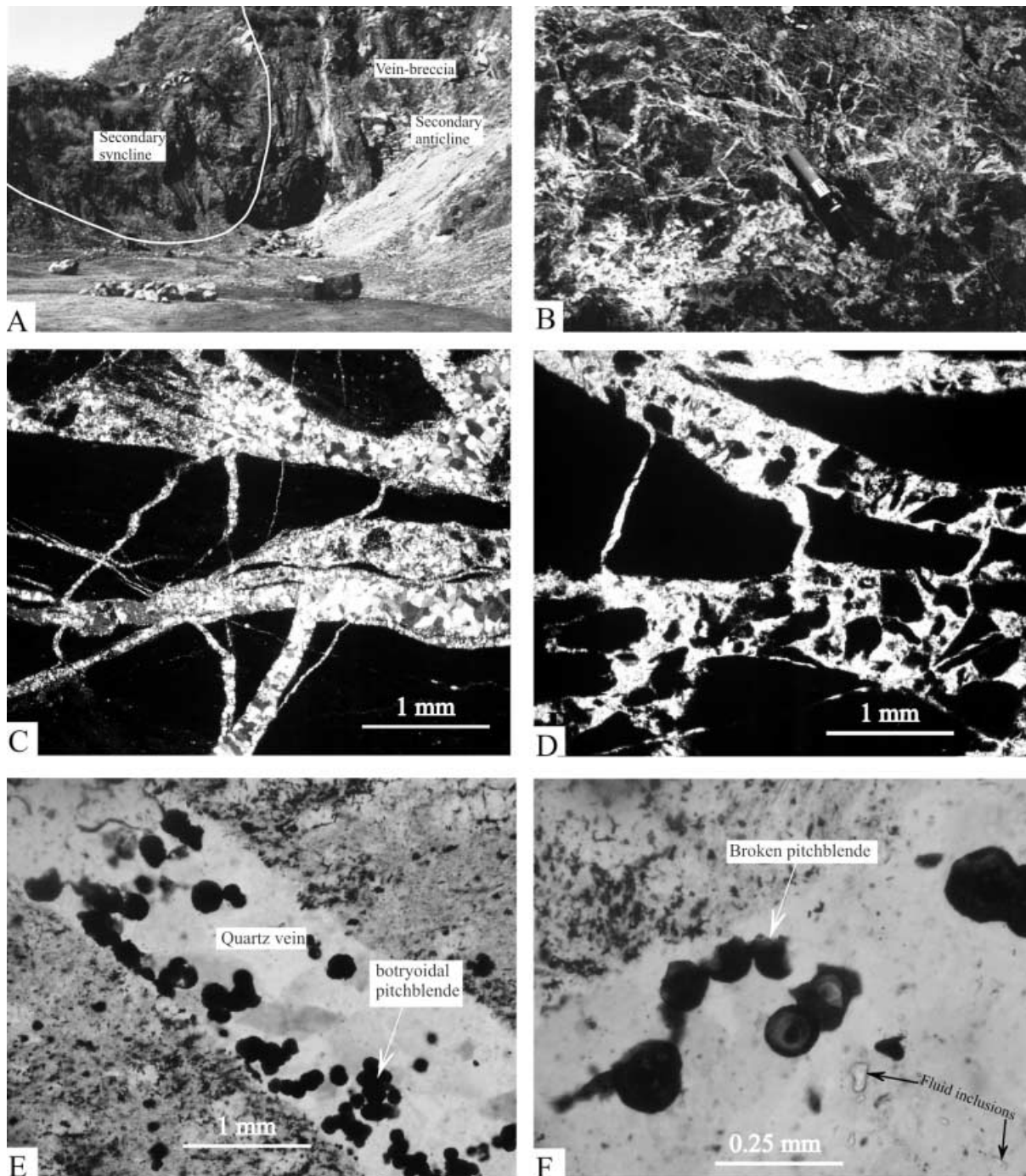
randomly cut the quartz crystals to form a microfracture network. No evidence for the presence of immiscible fluids or CO_2-rich fluids was found.

Microthermometry

Microthermometric analyses were performed on 52 primary and 5 secondary inclusions from both uranium-bearing and uranium-barren quartz samples, using methods described by Roedder (1976). The primary inclusions measured were dominantly liquid-rich, relatively regular in shape, and at least 8 μm in diameter. Only five secondary inclusions were measured because secondary inclusions are generally too small for accurate determination. The precision of the heating and cooling temperature determinations is 1–2 °C and 0.1 °C, respectively. The reported homogenization temperature results are not corrected for pressure. Most primary inclusions homogenized to a liquid phase, whereas the secondary ones always homogenized to a vapor phase. Homogenization temperatures (T_h) of 150–260, 205–

Fig. 6 Photographs and photomicrographs of breccia-vein and pitchblende. **A** Emplacement of quartz veins and fragments in an anticline's core of outcrop scale. Note that few quartz veins occur in the syncline (*left*). The carbonaceous shales (*black*) may have acted as the impermeable seals facilitating fluid overpressure. **B** Photograph showing general geometry and texture of breccia-vein system. There are abundant voids within quartz veins (*light*) and fragments (*dark*). The fragments show typical in situ brecciation: no displacement, rotation and abrasion are observed. **C** Angular fragments of black shale with a sharp outline showing a jigsaw-puzzle pattern. The veins are composed of fine-grained anhedral quartz with increasing grain size towards the vein center. This structure suggests in situ fragmentation caused by abnormally high fluid pressure (e.g., Thompson et al. 1985). **D** Mosaic breccias with poorly sorted fragments of black shale floating in a matrix of quartz. **E** Disseminated botryoidal pitchblende within a quartz vein. **F** Broken pitchblende, presumably suggestive of repeated hydraulic fracturing; also shown are some primary fluid inclusions in a quartz vein

respectively (Table 1 and Fig. 8). There is no obvious variation with depth in the T_h values.

The salinity of inclusions was calculated from ice-melting temperatures (T_{mi}) using the equations proposed by Potter et al. (1978). The T_{mi} values are commonly interpreted as maximum apparent salinity because of the possible presence of dissolved CO_2 in inclusion fluids (Hendenquist and Henley 1985a). However, because no independent CO_2 phase was identified in this study, the estimates of salinity should be relatively precise. The T_{mi} of the inclusions are between –3.4 and –9.5 °C, yielding salinities ranging from 5.6 to 13.4 and from 7.2 to 8.0 wt% NaCl equivalent, respectively, for the primary and secondary inclusions (Table 1). The salinity of the fluid inclusions appears to increase with decreasing T_h (Fig. 8).

280, and 170–235 °C were obtained for primary inclusions in uranium-bearing veins (stage 2), uranium-barren quartz veins (stage 1), and secondary inclusions,

Fig. 7 Paragenesis of the uranium ores. Also shown is the diagenetic and alteration mineralogy of the host rocks of the Dangchong Formation

Structural evolution	Stable depositional environment	Strike-slip faulting (Transpressional)	Hydraulic fracturing under transtensional regime			Uplift and erosion
Geologic time	Middle Permian	Jurrasic	Late Cretaceous to early Tertiary			Late Tertiary to Quaternary
Event	Diagenesis of the Dangchong Formation; uranium pre-enrichment	Emplacement of granites; regional silicification of rocks of the Danchong Formation	Hydrothermal uranium mineralization			Oxidation of primary ores
			Stage 1	Stage 2	Stage 3	
Quartz	——		————		——	
Chalcedony	– – –	– – – ·		——————		
Kaolinite	– – – –	– – – ·	– – – ·			
Illite	——					
Organic matter	– – – –					
Muscovite	– – – ·					
Biotite	– – – ·					
Chlorite		– – – ·				
Sericite		——	—			
Pyrite	– – – ·	– – – ·	——————			
Molybdenite			————			
Chalcopyrite			——			
Pitchblende				————————	– – ·?	
Marcasite				– – – ·		
Greenockite				– – – ·		
Galena				————————		
Sphalerite				———————		
Fluorite				– – – –		
Calcite		– – –		—————	—	
Hematite					——————	
Uronophane						– – – – –
Uranophilite						– – – – –
Torbernite						– – – – –
Zeunerite						– – – – –
Limonite						– – – – –

Table 1 Fluid inclusion data from the Sanerlin uranium deposit

Sample no.	Number of inclusions studied	Shape of inclusion	Vapor fraction (vol%)	Inclusion size (μm)	T_h (°C)	Homogenized phase	T_{mi} (°C)	Salinity (wt% NaCl equivalent)
Primary								
U180	2	a	10–20	6–11	168–190	Liquid	−5.3∼−7.0	8.3–10.5
B180	3	a and b	20–55	7–10	208–225	Liquid, vapor	−5.2∼−6.2	8.1–9.5
U130_1	4	a	15–25	5–16	156–231	Liquid	−6.4∼−9.5	9.7–13.4
U130_2	4	a and c	10–35	5–8	154–175	Liquid	−3.6∼−6.7	5.8–10.1
U130_3	3	c	15–25	8–10	155–172	Liquid	−5.4∼−9.1	8.4–13.0
B130	3	c	35–50	8–12	213–275	Liquid, vapor	−6.1∼−6.7	9.3–10.1
U80_1	3	b and c	25–30	5–7	150–153	Liquid	−4.9∼−5.7	7.7–8.8
U80_2	2	d	30–45	6–7	156–176	Liquid, vapor	−4.7∼−6.7	7.5–10.1
U30_1	2	a	25–50	10–11	166–174	Liquid	−4.7∼−7.9	7.4–11.6
U30_2	2	a	20–40	6–8	158–200	Liquid	−3.6∼−5.0	5.9–7.8
U-20	1	a	35	20	170	Liquid	−4.7	7.4
B-20	4	b and c	50–60	5–10	222–280	Liquid, vapor	−3.4∼−4.5	5.6–7.2
U-70	3	a and d	40–55	6–18	218–260	Liquid, vapor	−3.8∼−5.4	6.5–8.4
U-120	1	a and c	25–35	8–13	195	Liquid	−5.7∼−8.1	8.8–11.9
B-70	4	b and c	15–40	5–9	205–260	Liquid	−4.4∼−4.6	7.1–7.3
U-120	2	c	30–40	10–12	215–265	Liquid	−4.5∼−5.6	7.2–8.7
B-120	3	a and d	20–45	8–10	213–265	Liquid	−5.4∼−6.9	8.4–10.4
B-170	3	b	15–25	12–14	272–276	Liquid	−5.4∼−7.4	8.4–11.0
B-220	4	a	30–40	7–11	225–278	Liquid	−4.6∼−5.5	7.3–9.5
Secondary								
B180	1	a	65	6	210	Vapor	−4.7	7.4
U130_2	1	a	75	8	202	Vapor	−4.9	7.7
U80_2	1	a	60	5	170	Vapor	−5.1	8.0
U-20	1	a	80	6	198	Vapor	−4.8	7.6
B-20	1	a	85	9	235	Vapor	−4.5	72

Sample no. abbreviations: *U180* uraniferous quartz sample at 180 m level; *B-20* barren quartz sample at –20 m level; all uraniferous samples belong to stage 2, whereas barren samples are of stage 1. Inclusion shapes: *a* irregular; *b* elongate; *c* elliptical; *d* negative, crystal face

Fluid pressure estimation

Fluids from the Sanerlin deposit are considered to be within the H_2O–NaCl system. Roedder and Bodnar (1997) calculated isochores for H_2O–NaCl inclusions with salinities of ≤ 25 wt% NaCl, using the equations of Bodnar and Vityk (1994). Fluid pressure can be read from their isochores if the salinity and homoge-
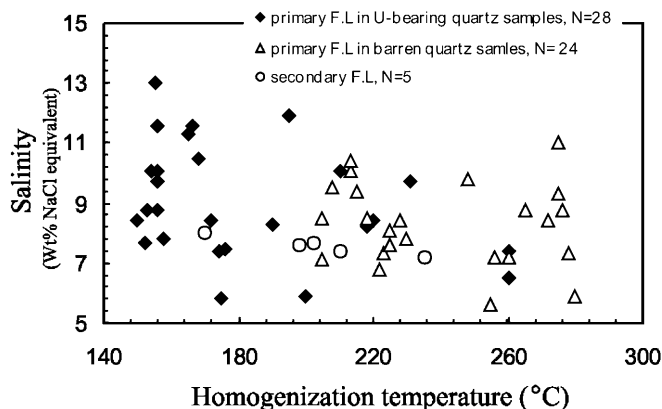

Fig. 8 Homogenization temperatures versus salinities for the analyzed fluid inclusions (F.L.) in quartz veins. The unusual correlation between salinity and T_h is discussed in the text

nization temperatures are known and if an independent geothermometer is available. We estimated the mineralization temperature using the oxygen isotope composition of coexisting quartz and calcite from the breccia-vein system. The only oxygen isotopic measurements of calcite in Sanerlin were conducted by Hou et al. (1993), who analyzed three U-bearing calcite samples (stage 2) collected from the 80 m level and these yielded $\delta^{18}O$ values between 12.8 and 15.3‰ SMOW (average 14.0). The $\delta^{18}O$ of quartz from the same level and same mineralization stage is 16.3–17.5‰ (average 16.9; this work, see below). The isotopic geothermometric equation between the coexisting quartz and calcite (Faure 1986) is as follows:

$$\delta^{18}O_{quartz} - \delta^{18}O_{calcite} = 0.60 \times 10^6 \times T^{-2}$$

The calculated formation temperature of the mineral pair is about 200 °C. Thus, the fluid pressure would be > 360 bar according to the relationship of Roedder and Bodnar (1997).

Stable isotope geochemistry

Nine ore samples from the levels between + 180 and – 220 m (Table 1) were systematically analyzed for oxygen

Table 2 Oxygen and hydrogen isotope compositions of fluid inclusions from vein quartz

Sample	Sample description	T_h (°C) (min–max)/average (inclusion number)	$\delta^{18}O_{quartz}$(‰)	$\delta^{18}O_{H_2O}$(‰) (min, max)/average	δD_{H_2O}(‰)
U180	Uraniferous quartz vein at the 180 m level	(168–190)/179(2)	14.7	(0.9, 2.6)/1.6	−125
U80_1	Uraniferous quartz vein at the 80 m level	(150–153)/151(3)	16.5	(−2.2, −1.9)/−1.9	−132
U80_2	Uraniferous quartz vein at the 80 m level	(156–176)/166(2)	16.3	(−1.8, −0.3)/−1.1	−121
U-20	Uraniferous quartz vein at the −20 m level	(260–260)/260(1)	14.9	(0.5, 0.5)/0.5	−114
U-120	Uraniferous quartz vein at the −120 m level	(195–195)/195(1)	14.6	(−0.6, −0.6)/−0.6	−128
B180	Barren quartz vein at the 180 m level	(208–225)/215(3)	15.8	(1.4, 2.3)/1.8	−110
B-20	Barren quartz vein at the −20 m level	(220–280)/253(4)	13.4	(−0.3, 2.5)/1.3	−134
B-120	Barren quartz vein at the −120 m level	(213–265)/230(3)	14.0	(−0.1, 2.5)/0.9	−120
B-220	Barren quartz vein at the −220 m level	(225–278)/244(4)	12.7	(−0.8, 1.7)/0.2	−116

Uraniferous samples belong to stage 2; barren samples belong to stage 1. T_h homogenization temperature

and hydrogen isotope compositions, at the Yichang Institute of Geology and Mineral Resources using a Nuclide 3-inch 600 ratio mass spectrometer. Separation of quartz from ores was accomplished by handpicking without any chemical treatment. The quartz separates were analyzed for $\delta^{18}O$ and extracted fluid inclusion waters were analyzed for δD. To ensure adequate fluid for analyses, 5–6 g of quartz separate were crushed in copper tubes under vacuum. The analytical techniques used are essentially the same as those described in Taylor (1978) and involve the reaction of ground quartz powders with BrF_5. Results are reported in delta notation relative to SMOW. The overall analytical errors are on the order of 0.1 and 1‰ for oxygen and hydrogen isotopes, respectively.

The analytical results are presented in Table 2. The δD values of the inclusion fluids range from −134 to −110‰ (Table 2). These values are much lower than those of magmatic and metamorphic fluids, but similar to values of formation waters in North America (McKibben and Hardie 1997). The $\delta^{18}O$ values of the mineralizing fluid can be calculated using the quartz–water fractionation equation (Friedman and O'Neil 1977). Nine quartz samples yielded $\delta^{18}O$ values between 12.7 and 16.5‰ (Table 2). Based on the homogenization temperatures from microthermometric study of the fluid inclusions, the calculated average $\delta^{18}O$ values of water in equilibrium with the quartz would be −2.2 to +2.6‰.

Liu (1980) systematically analyzed 17 pyrite samples from the ores and 8 samples from the host rocks of the Dangchong Formation. Samples from the ores yielded $\delta^{34}S$ values ranging from −48.2 ∼ +7.2‰. The values of the samples from the Dangchong Formation are between −30.6 and +3.7‰. The overlapping ranges of $\delta^{34}S$ indicate that the sulfur is probably from the country rocks and biogenic in origin.

Discussion

Evidence for hydraulic fracturing

The breccia-vein system in the Sanerlin uranium deposit has long been thought to be a fault breccia (Liu 1980; Xiao et al. 1989) or solution-collapse breccia (Hou et al. 1993; Min et al. 1996). Based on the morphology, structure, and texture of the breccia-vein system and the estimated fluid pressures, we reinterpret the origin of the system as being formed by hydraulic fracturing.

The quartz veins in the Sanerlin deposit, with horsetail structures and zigzag or en echelon morphologies, form a randomly oriented vein network. These morphologies agree well with the numerical modeling results of vein geometry in a hydraulic fracturing system (Beach 1980). Very fine grained and anhedral quartz crystals suggest that they crystallized rapidly (Rohel 1981; Beaudoin and Schrijver 1989), which is consistent with rapid opening and filling of fractures (Gratier and Gamond 1990). The ubiquitous Tuttle's planes represented by secondary fluid inclusions within the quartz crystals provide additional evidence for formation of the breccia-vein system by hydraulic fracturing (Tuttle 1949; Ramsay and Huber 1987; Gauthier-Lafaye and Weber 1989).

Within the randomly oriented quartz vein network, there are many in situ fragments of wall rock with sharp boundaries. The fragments along with the veins take a spectacular jigsaw-puzzle pattern (Fig. 6B–D), with the silicified fragments appearing to be floating in the hydrothermal matrix. In this case, both the brecciation and the hydrothermal quartz are interpreted to have been generated under abnormally high fluid pressures (e.g., Jobson et al. 1994). The presence of fractured and bro-

ken pitchblende (Fig. 6F) further convincingly suggests that repeated hydraulic fracturing accompanied mineralization. Abundant voids occurring in the fragments and hydrothermal cements, and the correlation of void abundance with the size and roundness of fragments, indicate abrupt release of gaseous phases.

Nineteen quartz samples collected over a vertical extent of more than 500 m yield homogenization temperatures essentially indistinguishable from one another, indicating that the mineralizing fluids were transported upwards very quickly. Craw and Mckeag (1995) proposed that velocities could be as great as 530 m/s for waters at 200 °C and moving upward in a straight conduit under a hydraulic fracturing regime. The salinity of the fluid inclusions appears to increase with decreasing T_h (Fig. 8), which is not the case for most hydrothermal ore deposits. We interpret this to be the result of significant vapor loss from the hydrothermal solutions during hydraulic fracturing. Vapor loss in gas-rich fluids leads to substantial increase in salinity because salts are strongly partitioned into the liquid phase (Hedenquist and Henley 1985a). Therefore, the high salinity of inclusions may represent the trapping of a late residual fluid after gas loss (with lower temperature relative to its counterpart before vapor loss occurred) as a response to hydraulic fracturing. Such a correlation between salinity and temperature has also been identified in some geothermal fields (Ruggieri et al. 1997) and uncommonly in hydrothermal ore deposits (Ahmad 1993), where hydraulic fracturing has been shown to have occurred.

Possible mechanism for hydraulic fracturing

Hydraulic fracturing can occur at depths of several to more than 10 km, especially under an extensional tectonic regime (Fyfe et al. 1978; Richards 1992; Ruggieri and Gianelli 1999), as is the case in the Sanerlin area from the Cretaceous to early Tertiary (Xu et al. 1987). Hydraulic fracturing requires abnormally high fluid pressures. The critical fluid pressures necessary for hydraulic fracturing (P_f) in extensional tectonic regimes can be calculated using the equation proposed by Hubbert and Willis (1957):

$$P_f \approx \left(P_{lith} + 2P_{hydro}\right)/3$$

Based on the amount of erosion of the study area since the late early Tertiary, the brecciation and uranium mineralization at Sanerlin were estimated to have occurred at depths of 1,500 to 2,200 m (Li 1998). We adopt an average density of 2.7 g/cm^3 for the overlying rocks, yielding lithostatic (P_{lith}) and hydrostatic (P_{hydro}) pressures of about 397–582 and 147–216 bar, respectively. Accordingly, the calculated fluid pressure values required for hydraulic fracturing are 230–338 bar. Thus, the fluid pressures estimated from the fluid inclusion data (> 360 bar) are sufficient to facilitate hydraulic fracturing.

Impermeable seals are required for the development of fluid overpressure. In the Sanerlin deposit, the shale-dominated Dangchong Formation has acted as an impermeable seal. Silicification of these rocks further enhanced the impermeability and competent nature of the strata. The cores of the anticlines may have provided favorable sites for fluid accumulation to form geopressured (overpressured) zones. The Cretaceous–early Tertiary transtensional regime exerted by the Chaling–Yongxing and Chenxian–Linwu faults created an abnormal regional heat flux and permeable fault network in the pull-apart stepover area between these strike-slip faults (e.g., Sibson 1987; Willis and Tosdal 1992), providing sufficient waters and heat supply necessary for hydraulic fracturing. Existence of an elevated geothermal gradient in the study area is supported by the occurrences of several modern hot springs, individually with temperatures as high as 72 °C and flow capacity of as much as 15 l/s, along the Chaling–Yongxing and Chenxian–Linwu faults.

Moderate increases in temperature would produce large increases in fluid pressure in a relatively closed system (Knapp and Knight 1977). Thus, the accumulation of hydrothermal fluids in the cores of secondary
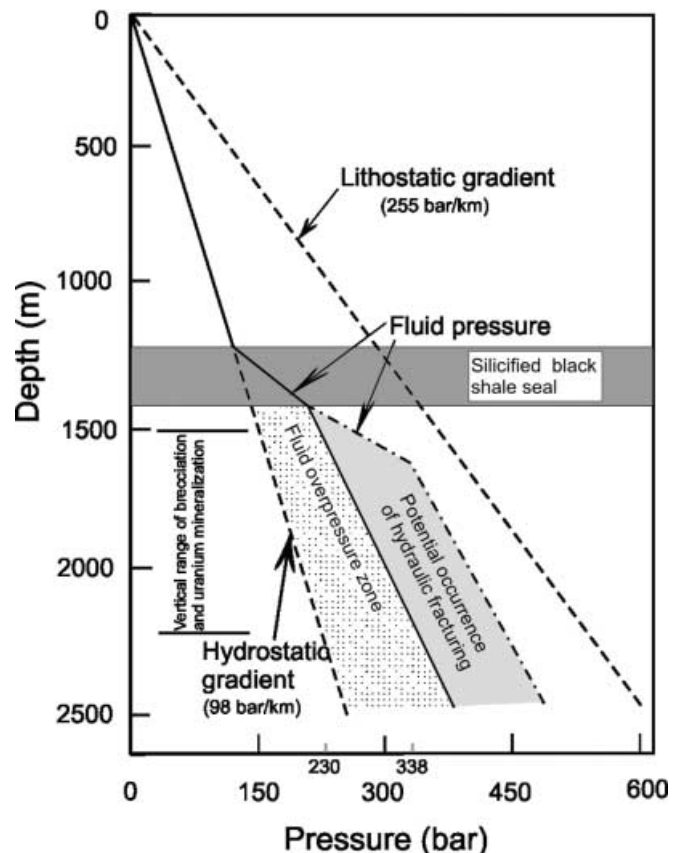

Fig. 9 Possible development of fluid overpressure under the geological conditions (with impermeable seals) that existed in the area of the Sanerlin deposit. (Modified from Hedenquist and Henley 1985b; Gauthier-Lafaye and Weber 1989; Branquet et al. 1999)
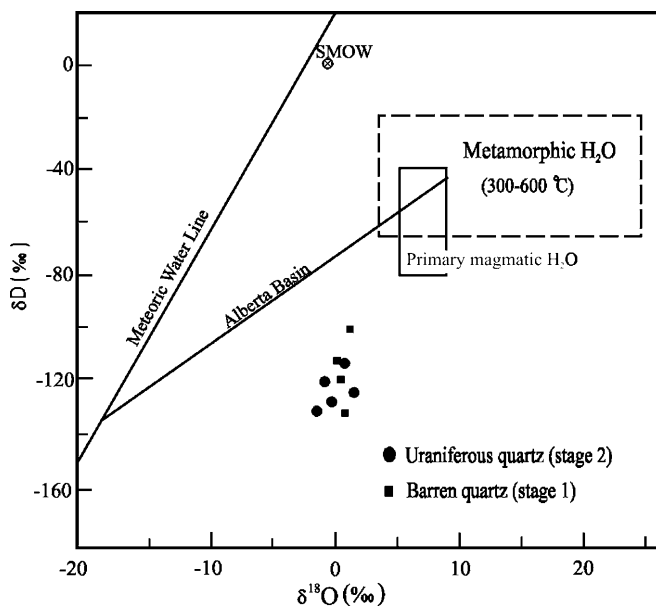
Fig. 10 Diagram of δD versus δ^{18}O for the mineralizing fluids

anticlines would have caused a buildup of the fluid pressure due to the overlying impermeable seal (Fig. 9). Hydraulic fracturing and brecciation ensued when the increased fluid pressure exceeded the rock strength (Ramsay and Huber 1987). This caused oversaturation of the mineralizing solution due to an abrupt decrease of temperature and pressure, consequently leading to precipitation of quartz, pitchblende, and associated minerals from the fluids (e.g., Vrolijk 1987). However, movement on the strike-slip faults may also have induced some of the hydraulic fracturing and brecciation.

Origin of the Sanerlin uranium deposit

Previous geochronological studies by the conventional U–Pb dating method have yielded the concordant ages of 13 pitchblende samples from the Sanerlin deposit at 62.8 to 60.1 Ma (Liu 1980). The early Tertiary time of uranium mineralization in the study area coincides with the transtensional regime along the regional strike-slip fault system and the formation of the Chaling–Yongxing basin. The gypsum beds and red beds in this pull-apart basin suggest an arid and oxidizing climate in the Cretaceous and early Tertiary. Hydrogen and oxygen isotope compositions of the ores indicate that the mineralizing fluids were largely derived from oxidizing basinal formation waters (Fig. 10). This idea has been further supported by the salinity of fluids in the Sanerlin deposit, which is similar to that of formation waters of continental sedimentary basins (e.g., Ferguson et al. 1993). Oxidizing waters were efficient for leaching and transporting uranium and other metals from the black shales (cf. Rich et al. 1977). The arid climate was also conducive to uranium mobilization from the uranium-bearing granites

south and north of the Sanerlin deposit by supergene processes and ground waters (Dahlkamp 1993), which could be additional source areas for the uranium.

The deep strike-slip faults that cut through the Sanerlin area are about 200 km long and estimated slip is 1 km (Rao 1993; Li 1998). The volume of fluid that could be concentrated in the pull-apart stepover would be $10^{12} \sim 10^{13}$ m^3 according to the relationship in Sibson et al. (1975). Based on experimental results of quartz solubility (Holland 1967), such fluid volumes at 300 °C and 300 bar (similar to the fluid conditions of the Sanerlin deposit) can potentially dissolve $\sim 10^{16}$ g of quartz as well as other minerals from crustal rocks. Because the solubility of quartz in hot water depends largely on temperature and pressure (Holland 1967), the abrupt P–T drop of the hydrothermal system due to hydraulic fracturing could have caused fluid unmixing, and resultant precipitation of quartz to form the vein network. Pitchblende and associated metallic minerals were deposited almost simultaneously with the quartz.

The black shales of the Dangchong Formation are potentially the most significant uranium source rocks. These shales are rich in clays and organic materials such as algae, organic carbon, and coal and lignite, all of which have been documented to be significant agents for uranium pre-enrichment by adsorption and reduction (Rich et al. 1977; Boyle 1982; Dahlkamp 1993; Min 1995; Min et al. 1997). Chemical analysis of 118 samples show that rocks of the Dangchong Formation have an average uranium content of 34 ppm, as much as 180 ppm in the black carbonaceous shales (Liu 1980) (Fig. 3). The similar sulfur isotope compositions of pyrite from the ores and from rocks of the Dangchong Formation support rocks of the Dangchong Formation as being the most important source of uranium.

Conclusions

Based upon our interpretations of geology, alteration, and geochemical data, we conclude that the Sanerlin uranium deposit formed by the following steps: (1) pre-enrichment of uranium in rocks of the Dangchong Formation facilitated by the abundant organic material and clay in the shales; (2) Early–Middle Jurassic transpression that generated granitic intrusions and caused NNE-trending folding; (3) Late Jurassic to early Tertiary transtension that resulted in the formation of the Chaling–Yongxing basin and an abnormally high geothermal gradient; (4) oxidized basinal formation waters dissolved uranium from the Dangchong Formation and the uranium was concentrated in the cores of secondary anticlines: the impermeable shales of the Dangchong Formation acted as the seals to the hydrothermal fluids that resulted in fluid overpressure; (5) hydraulic fracturing and brecciation occurred when increased fluid pressure exceeded the rock strength; and (6) quartz, pitchblende, and other associated minerals precipitated due to the P–T drop and release of gaseous phases from

the mineralizing fluids, caused by episodic hydraulic fracturing.

References

Ahmad M (1993) The origin of tin deposits in the Mount Wells region, Pine Creek Geosyncline, Northern Territory. Aust J Earth Sci 40:427–443

Beach A (1980) Numerical modes of hydraulic fracturing and the syntectonic veins. J Struct Geol 17:435–446

Beaudoin G, Schrijver K (1989) A vein and disseminated Ba–Pb–Zn deposit in the Appalachian Thrust Belt, St.-Fabien, Quebec. Econ Geol 84:799–816

Bodnar RJ, Vityk MO (1994) Interpretation of microthermometric data for H$_2$O–NaCl fluid inclusions. In: Vivo BD, Freaaotti ML (eds) Fluid inclusions in minerals, methods and applications. Virginia Polytechnic Institute, Blacksburg, pp 117–130

Bouchot V, Cros Y, Piantone P (1994) Dynamics of shallow late-Variscan gold mineralization: the Le Chatelet Au–arsenopyrite quartz veins, Massif Central, France. Miner Deposita 29:461–473

Boyle WW (1982) Geochemical prospecting for thorium and uranium deposits. Elsevier, Amsterdam

Branquet Y, Cheilletz A, Giuliani G, Laumonier B, Blanco O (1999) Fluidized hydrothermal breccia in dilatant faults during thrusting: the Colombian emerald deposits. In: McCaffery K, Lonergan L, Wilkinson J (eds) Fractures, fluid flow and mineralization. Geol Soc Lond Spec Publ 155, pp 183–196

Callan NJ, Spooner ETC (1998) Repetitive hydraulic fracturing and shear zone inflation in an Archean granitoid-hosted, ribbon banded, Au–quartz vein system, Renabie area, Ontario, Canada. Ore Geol Rev 12:237–266

Cox SF (1995) Faulting process at high fluid pressure: an example of fault valve behaviour from the Wattle Gully Fault, Bitoria, Australia. J Geophys Res 100B:12831–12850

Craw D, Mckeag SA (1995) Structural control of Tertiary Au–Ag-breccias in an extensional environment, Nelson area, Southern Nevada, USA. Miner Deposita 30:1–20

Dahlkamp FJ (1993) Uranium ore deposits. Springer, Berlin Heidelberg New York, pp 89–92

Etheridge MA, Wall VJ, Cox SF (1983) High fluid pressure during regional metamorphism and deformation: implication for mass transport and deformation mechanism. J Geophys Res 89B:4344–4358

Faure G (1986) Principles of isotope geology, 2nd edn. Wiley, Singapore, pp 460–465

Ferguson J, Etminan H, Ghassemi F (1993) Geochemistry of deep waters in the Canning Basin, Western Australia, and their relationship to Zn–Pb mineralization. Aust J Earth Sci 40:471–483

Friedman I, O'Neil JR (1977) Compilation of stable isotopes fractionation factors of geothermal interest. US Geol Surv Prof Paper 440-KK

Fyfe WS, Price NJ, Thompson AB (1978) Fluids in the Earth's crust. Elsevier, Amsterdam, pp 259–266

Gauthier-Lafaye F, Weber F (1989) The Francevillian (Lower Proterozoic) uranium deposits of Gabon. Econ Geol 84:2267–2285

Gilder SA, Gill J, Coe RS, Zhao XX, Liu ZZ, Wang GX, Yuan KR, Liu WL, Kuang GD, Wu HR (1996) Isotopic and paleomagnetic constraints on the Mesozoic tectonic evolution of south China. J Geophys Res 101B:16137–16154

Gratier JP, Gamond JF (1990) Transition between seismic and aseismic deformation in the upper crust. In: Knipe RJ, Rutter EH (eds) Deformation mechanisms, rheology and tectonics. Geol Soc Lond Spec Publ 54, pp 461–473

HB (Hunan Bureau of Geology and Mineral Resources) (1988) Regional geology of Hunan Province, south China (in Chinese with English summary). Geological Publishing House, Beijing

Hedenquist JW, Henley RW (1985a) The importance of CO$_2$ on freezing-point measurements of fluid inclusions: evidence from active geothermal systems and implications for epithermal ore deposition. Econ Geol 80:1379–1406

Hedenquist JW, Henley RW (1985b) Hydrothermal eruptions in the Waiotapu geothermal system, New Zealand: their origin, associated breccias and relation to precious metal mineralization. Econ Geol 80:1640–1668

Henley RH, Adams DPM (1992) Strike-slip fault reactivation as a control on epithermal vein-style gold mineralization. Geology 20:443–446

Holland HD (1967) Gangue minerals in hydrothermal deposits. In: Barnes HL (ed) Geochemistry of hydrothermal ore deposits. Holt, Rinehart & Winston, New York, pp 382–436

Hou YQ, Wang QH, Liu LJ (1993) Genesis and prospecting direction of the no. 320 uranium deposit (in Chinese with English abstract). Uranium Geol 9:6–13

Hsü KJ, Li JL, Chen HH, Wang QC, Sun S, Sengor AMC (1990) Tectonics of south China: key to understanding west Pacific geology. Tectonophysics 183:9–39

Hubbert MK, Willis DG (1957) Mechanics of hydraulic fracturing. Trans Am Inst Mech Eng 210:153–168

Jahn BM, Zhou XH, Li JL (1990) Formation and tectonic evolution of southeastern China and Taiwan: isotopic and geochemical constraints. Tectonophysics 183:145–160

Jobson DH, Boulter GA, Foster RP (1994) Structural controls and genesis of epithermal gold-bearing breccias at the Lebong Tandai mine, Western Sumatra, Indonesia. J Geochem Explor 50:409–428

Knapp RB, Knight JE (1977) Differential thermal expansion of pore fluids: fracture propagation and microearthquake production in hot pluton environments. J Geophys Res 82:2515–2521

Li JW (1998) The NNE-trending strike slip faulting, fluid flow and uranium mineralization in the border area between Hunan and Jiangxi Provinces, southern China(in Chinese with English summary). PhD Thesis, China University of Geosciences

Li JW, Zhou MF, Li XF, Fu ZR, Li ZJ (2001) The Hunan–Jiangxi strike-slip fault system in South China: southern extension of the Tan-Lu fault. J Geodyn 32:333–354

Liu SL (1980) The genetic mechanisms of no. 320 uranium deposit (in Chinese). Radioactiv Geol 2:97–108

Mathis V, Robert JP, Saint MJ (1990) Géologie et métallogénie des gisements d'uranium du basin permien de Lodève (sud du Massif central francais). Chron Rech Miner 499:31–40

McKibben MA, Hardie LA (1997) Ore-forming brines in active continental rifts. In: Barnes HL (ed) Geochemistry of hydrothermal ore deposits. Wiley, New York, pp 877–936

Min M (1995) Carbonaceous–siliceous–pelitic rock type uranium deposits in southern China: geologic setting and metallogeny. Ore Geol Rev 10:51–64

Min MZ, Wang XY, Shen BP (1996) Mechanics of the mineralized breccias in no. 320 uranium deposit (in Chinese with English abstract). Uranium Geol 12:24–28

Min MZ, Zheng DY, Shen D, Wen G, Gandhi SS (1997) Genesis of the Sanbaqi deposit: a palaeokarst-hosted uranium deposit in China. Miner Deposita 32:505–519

Phillips WJ (1972) Hydraulic fracturing and mineralization. J Geol Soc Lond 128:337–359

Potter RW II, Clynne MA, Brown DL (1978) Freezing point depression of aqueous sodium chloride solutions. Econ Geol 73:284–285

Ramsay JG (1980) The crack-seal mechanism of rock deformation. Nature 284:135–139

Ramsay JG, Huber M (1987) The techniques of modern structural geology. Academic Press, London, pp 577–585

Rao JR (1993) Deep structure and tectonics of Hunan province (in Chinese with English abstract). Hunan Geol Suppl 7:18–70

Rich RA, Holland HD, Peterson U (1977) Hydrothermal uranium deposits. Elsevier, Amsterdam, pp 54–72

Richards JR (1992) Magmatic–epithermal transitions in alkalic systems: Porgera gold deposit, Papua New Guinea. Geology 20:547–550

Roedder R (1976) Fluid inclusion evidence of the genesis of ores in sedimentary and volcanic rocks. In: Wolf KH (ed) Handbook of stratabound and stratiform ore deposits. Elsevier, New York, pp 67–110

Roedder R (1984) Fluid inclusions. Rev Mineral 12:644

Roedder E, Bodnar RJ (1997) Fluid inclusion studies of hydrothermal ore deposits. In: Barnes HL (ed) Geochemistry of hydrothermal ore deposits. Wiley, New York, pp 679–681

Rohel PO (1981) Dilation breccias – a proposed mechanism of fracturing, petroleum expulsion and dolomitization in the Monterey Formation, California. In: Garisosn RE, Douglas RC (eds) The Monterey Formation and the related siliceous rocks of California. Soc Econ Paleont Mineral Sym, Pacific Section, Los Angeles, pp 285–315

Ruggieri G, Gianelli G (1999) Multi-stage fluid circulation in a hydraulic fracturing breccia of the Larderello geothermal field (Italy). J Volcanol Geotherm Res 90:241–261

Ruggieri G, Lattanzi P, Luxoco SS, Dessi R, Benvenuti M, Tanelli G (1997) Geology, mineralogy and fluid inclusion data of the Furtei high-sulphidisation gold deposit. Econ Geol 92:1–19

Sibson RH (1987) Earthquake rupturing as a mineralizing agent in hydrothermal systems. Geology 15:701–704

Sibson RH, Moore JMC, Rankin AH (1975) Seismic pumping – a hydrothermal fluid transport mechanism. J Geol Soc Lond 131:653–659

Sillitoe RH (1985) Ore-related breccias in volcanoplutonic arcs. Econ Geol 80:1467–1514

Spirakis CC, Pierson CT (1986) Some aspects of the genesis of uranium deposits of the Morrison Formation in the Grants Uranium Region, New Mexico, inferred from chemical characteristic of the deposits. In: Turner-Peterson CE, Santos ES, Fishman NS (eds) A basin analysis case study – the Morrison Formation, Grants Uranium Region, New Mexico. Am Assoc Petrol Geol, Stud Geol 22:161–169

Taylor HP (1978) The application of oxygen and hydrogen isotope studies to problems of hydrothermal alteration and ore deposition. Econ Geol 69:843–883

Thompson TB, Trippel AD, Dwelley DC (1985) Mineralized veins and breccias of the Cripple Creek District, Colorado. Econ Geol 80:1669–1688

Tuttle OF (1949) Structural petrology of planes of liquid inclusions. J Geol 57:331–356

Vrolijk PJ (1987) Tectonically-driven fluid flow in the Kodiak accretionary complex, Alaska. Geology 15:466–469

Willis GF, Tosdal RM (1992) Formation of gold mines and breccias during dextral strike-slip faulting in the Mesquite mining district, southern California. Econ Geol 87:2002–2022

Xiao J, Han LS, Tang DL (1989) The genesis of the silicified zones in southern Hunan province and their ore-prospecting significance (in Chinese with English abstract). Miner Deposits 8:70–75

Xu JW, Zhu G, Tong WX (1987) Formation and evolution of the Tancheng–Lujiang wrench fault system: a major shear system to the northwest of the Pacific Ocean. Tectonophysics 134:273–310